Current Research in Toxicology 6 (2024) 100172

Contents lists available at ScienceDirect

Current Research in Toxicology

journal homepage: www.journals.elsevier.com/current-research-in-toxicology

Research Paper

Acute toxicity of binary mixtures for quorum sensing inhibitors and sulfonamides against *Aliivibrio fischeri*: QSAR investigations and joint toxic actions

Zhenheng Long [a], Jingyi Yao [a], Minghong Wu [a], Shu-shen Liu [b], Liang Tang [a,*], Bo Lei [a], Jiajun Wang [a], Haoyu Sun [a,c,*]

[a] *Key Laboratory of Organic Compound Pollution Control Engineering (MOE), School of Environmental and Chemical Engineering, Shanghai University, Shanghai 200444, China*
[b] *State Key Laboratory of Pollution Control and Resource Reuse, College of Environmental Science and Engineering, Tongji University, Shanghai 200092, China*
[c] *Shandong Key Laboratory of Environmental Processes and Health, School of Environmental Science and Engineering, Shandong University, Qingdao 266237, China*

ARTICLE INFO

Keywords:
Quorum sensing inhibitors
Sulfonamides
Acute toxicity
QSAR
Joint toxic action
Bioluminescence

ABSTRACT

Quorum sensing inhibitors (QSIs), as a kind of ideal antibiotic substitutes, have been recommended to be used in combination with traditional antibiotics in medical and aquaculture fields. Due to the co-existence of QSIs and antibiotics in environmental media, it is necessary to evaluate their joint risk. However, there is little information about the acute toxicity of mixtures for QSIs and antibiotics. In this study, 10 QSIs and 3 sulfonamides (SAs, as the representatives for traditional antibiotics) were selected as the test chemicals, and their acute toxic effects were determined using the bioluminescence of *Aliivibrio fischeri* (*A. fischeri*) as the endpoint. The results indicated that SAs and QSIs all induced S-shaped dose-responses in *A. fischeri* bioluminescence. Furthermore, SAs possessed greater acute toxicity than QSIs, and luciferase (Luc) might be the target protein of test chemicals. Based on the median effective concentration (EC_{50}) for each test chemical, QSI-SA mixtures were designed according to equitoxic ($EC_{50(QSI)}$:$EC_{50(SA)}$ = 1:1) and non-equitoxic ratios ($EC_{50(QSI)}$:$EC_{50(SA)}$ = 1:10, 1:5, 1:0.2, and 1:0.1). It could be observed that with the increase of QSI proportion, the acute toxicity of QSI-SA mixtures enhanced while the corresponding TU values decreased. Furthermore, QSIs contributed more to the acute toxicity of test binary mixtures. The joint toxic actions of QSIs and SAs were synergism for 23 mixtures, antagonism for 12 mixtures, and addition for 1 mixture. Quantitative structure–activity relationship (QSAR) models for the acute toxicity QSIs, SAs, and their binary mixtures were then constructed based on the lowest CDOCKER interaction energy ($E_{\text{bind-Luc}}$) between Luc and each chemical and the component proportion in the mixture. These models exhibited good robustness and predictive ability in evaluating the toxicity data and joint toxic actions of QSIs and SAs. This study provides reference data and applicable QSAR models for the environmental risk assessment of QSIs, and gives a new perspective for exploring the joint effects of QSI-antibiotic mixtures.

1. Introduction

The abuse of antibiotics has contributed to the severe problem of bacterial resistance, which threatens the ecological environment and human health (Darby et al., 2023; Shao et al., 2021). Seeking ideal antibiotic alternatives is regarded as an effective strategy for controlling the wide spread of bacterial resistance. Quorum sensing inhibitors (QSIs), as a kind of new antibiotics, take the quorum sensing (QS) of bacteria as the target (Kalia, 2013; Zhou et al., 2020). They could interfere with biofilm formation, virulence factor production, or pathogenic gene expression (Carradori et al., 2020; Cui et al., 2020). Due to the low selection pressure on microbial growth, QSIs are considered to

Abbreviations: QSIs, quorum sensing inhibitors; SAs, sulfonamides; *A. fischeri*, *Aliivibrio fischeri*; QSAR, quantitative structure–activity relationship; 22D3F, 2,2-Dimethyl-3(2H)-furanone; 2F, 2(5H)-Furanone; 2M3F, 2-Methyltetrahydro-3-furanone; B3O, Benzofuran-3(2H)-one; S5H2F, (S)-(−)-5-Hydroxymethyl-2(5H)-furanone; γV, γ-Valerolactone; 1P1C, 1-Pyrrolidino-1-cyclohexene; R3P, (R)-3-Pyrrolidinol; S2P, (S)-(+)-2-Pyrrolidinemethanol; 2P5CA, 2-Pyrrolidone-5-carboxylic acid; SCP, sulfachloropyridazine; SIX, sulfisoxazole; SMX, sulfamethoxazole.

* Corresponding authors at: School of Environmental and Chemical Engineering, Shanghai University, 333 Nanchen Road, Shanghai 200444, China.
E-mail addresses: tang1liang@shu.edu.cn (L. Tang), sunhaoyu2021@shu.edu.cn (H. Sun).

https://doi.org/10.1016/j.crtox.2024.100172
Received 26 December 2023; Received in revised form 8 May 2024; Accepted 9 May 2024
Available online 10 May 2024

be suitable antibiotic substitutes for protecting humans, economical crops, and aquatic organisms from pathogens (Díaz et al., 2020; Kalia et al., 2019). Furthermore, QSIs have been recommended to be used in combination with traditional antibiotics, which could not only enhance the antibacterial efficacy of QSIs but also reduce the usage of traditional antibiotics (Bai et al., 2022; Ning et al., 2021). Therefore, QSIs and antibiotics possibly enter environmental media simultaneously, and exist as a mixture form (Li et al., 2021). The joint effects of QSIs and antibiotics should be paid enough attention in the fields of toxicology and environmental risk assessment.

Over the past several decades, a lot of researches have reported the joint effects of QSIs and antibiotics (such as sulfonamides (SAs), tetracyclines, quinolones, aminoglycosides, and other β-lactams) when setting bacteria as the test organisms (e.g., *Aliivibrio fischeri* (*A. fischeri*), *Escherichia coli*, *Pseudomonas aeruginosa*, *Vibrio cholerae*, *Staphylococcus aureus*) (Bernabè et al., 2021; Haque et al., 2021; Mangal et al., 2022; Odularu et al., 2022; Rezzoagli et al., 2020; Wang et al., 2016). However, these studies paid more attention to the antibacterial efficacy, and the corresponding toxicological evaluation was usually based on the chronic exposure. There is little information regarding the acute toxicity for the mixtures of QSIs and antibiotics. Acute toxicity could give the most comprehensive data of species sensitivity for chemicals or pollutants, which plays a pivotal role in environmental risk assessment (Wang and Wang, 2021). In China, USA, EU, and some other countries, acute toxicity data has been used as the fundamental parameter to estimate chemical's safety concentration and risk threshold when setting criteria about environmental protection or management (Naveira et al., 2021; Stubblefield et al., 2020; Yang et al., 2014). In addition, most toxicological studies usually focused on the fixed ratio of QSI and antibiotic in the mixture (Wang et al., 2018a; Wang et al., 2016). QSIs and antibiotics may co-exist at different ratios in the environment. Hence, it is necessary to investigate the acute toxicity for the mixtures of QSIs and antibiotics at different ratios, which will contribute to clarifying the environmental risk of their mixtures.

The luminescent bacteria *A. fischeri* has been widely used as the model organism in both acute and chronic toxicity assessments of chemicals (Abbas et al., 2018; Parvez et al., 2006), because its bioluminescence is sensitive to external changes, is convenient, and allows rapid evaluation (Mirjani et al., 2021). In previous studies, the hormetic effects of exogenous chemicals on *A. fischeri* bioluminescence have been frequently reported in chronic toxicity determination (Sun et al., 2020; You et al., 2016), which are characterized by low-dose stimulation and high-dose inhibition. These biphasic dose-responses are typically represented as J-shaped or inverted U-shaped curves (Agathokleous et al., 2023b; Calabrese et al., 2020). The hormetic phenomenon is challenging the central beliefs in the toxicity evaluation and environmental risk assessment of pollutants, including endpoint selecting, concentration-range setting, exposure time optimizing, and mechanism exploring (Agathokleous et al., 2023a; Agathokleous et al., 2023b). Moreover, mechanistic exploration reveals that the hormetic phenomenon of *A. fischeri* bioluminescence possibly results from the acting of exogenous chemicals on the QS system of bacteria (Sun et al., 2018), and the variation for the modes of actions of component with the dose contributes to the heterogenous pattern of joint toxic action for pollutant mixtures (Sun et al., 2018). Hence, it is crucial to explore if *A. fischeri* bioluminescence demonstrates hormetic phenomena when subjected to acute exposures of QSIs, antibiotics, and their mixtures. In addition, quantitative structure–activity relationship (QSAR) is an effective tool for linking chemical toxicity with molecular structure, which could not only predict the toxic effects of chemicals or mixtures but also provide convincing support for corresponding mechanistic exploration (Abramenko et al., 2020; Chatterjee and Roy, 2021; Yang et al., 2021). Therefore, the QSAR models could help to reveal the critical factors for the acute toxicity for the mixtures of QSIs and antibiotics, and meanwhile make their toxicity and risk estimation more convenient and efficient.

As typical QSIs, furanones, pyrroles, and pyrrolidones have been widely used in agriculture, medicine, and food industry (Husain et al., 2019; Jeelan et al., 2022). Here, six furanones, three pyrroles, and one pyrrolidone were selected as the test QSIs. SAs were set as the representatives for traditional antibiotics due to their common use in livestock breeding and frequent detection in the environment (Cheong et al., 2020; Zuo and Ai-yun, 2021). The objectives of this study were: (1) to determine the acute toxicity of single QSIs and SAs to *A. fischeri* bioluminescence and design their mixtures at equitoxic and non-equitoxic ratios; (2) to test the combined toxicity of QSIs and SAs; (3) to construct QSAR models for the individual and combined toxicity using suitable structural descriptors of QSIs and SAs and the component proportion in binary mixtures; and (4) to judge the joint toxic actions between QSIs and SAs at equitoxic and non-equitoxic ratios based on the observed values for the median effective concentration (EC_{50}) and the predicted EC_{50} values from the QSAR models.

2. Materials and methods

2.1. Chemicals and organism

10 QSIs and 3 SAs were purchased from Sigma-Aldrich co. LLC. (St. Louis, MO, USA). Table 1 lists their detailed information. The test chemicals were diluted with 2 % (*w/v*) NaCl solution to appropriate concentrations for toxicity test. DMSO was used to improve the solubility of chemicals, and the final concentration of DMSO was less than 0.1 % (*v/v*) in the diluted samples. *A. fischeri* (ATCC7744) was bought from the American Type Culture Collection (Manassas, VA, USA). The freeze-dried bacterium was then reconstituted and maintained on agar slants at 4 °C. The F3 generation was used in subsequent tests to guarantee the adequate cell viability and stable bioluminescence.

2.2. Toxicity determination

The acute toxicity of test chemicals on *A. fischeri* bioluminescence were measured using the microplate toxicity assay (Sun et al., 2020). Previous studies have indicated that the residual level of SAs exceed 1 μg/L in some rivers and lakes (Kergoat et al., 2021; Kulik et al., 2023). With the constant application of QSIs, their environmental concentrations will be at non-negligible levels (Shen et al., 2021). Based on the environmental residual, the application prospect, and the results from preliminary experiment, the test concentrations for QSIs and SAs were set as listed in **Table S1**. In each test, there were 16 concentration points with fixed equal log dose interval between adjacent concentrations. Each well contained 80 μL test chemical, 80 μL 2 % (*w/v*) NaCl solution, and 40 μL readily prepared *A. fischeri*. The control group was prepared by replacing the test chemical with 2 % (*w/v*) NaCl solution. All treatment and control groups were conducted in quintuplicate. The non-transparent 96-well microplate was then incubated at 22 °C for 15 min, and the relative light unit (RLU) was determined on Mithras LB 940 microplate reader (Berthold Technologies, Germany). The inhibition of test chemical on *A. fischeri* bioluminescence was calculated as:

$$\text{Inhibition (\%)} = \left(1 - \frac{I_t}{I_c}\right) \times 100\% \tag{1}$$

where I_t and I_c respectively were the average RLU values in the treatment and control groups. The EC_{50} value for each chemical was then computed based on the decrease in RLU using a probit model. The binary mixtures of QSIs and SAs were designed according to the equitoxic ratio ($EC_{50(QSI)}$:$EC_{50(SA)}$ = 1:1) and non-equitoxic ratios ($EC_{50(QSI)}$:$EC_{50(SA)}$ = 1:10, 1:5, 1:0.2, and 1:0.1) of EC_{50} values for single chemicals (Hamid et al., 2020; Tian et al., 2013), and their combined toxicity was tested using the above method. The test concentrations for each binary mixture are shown in **Table S2**.

Table 1
Detailed information on the test chemicals.

Class	Chemical name	Abbreviation	CAS	Structure	Relative molecular weight (g/mol)	Mean EC_{50} ± SD[a] (mol/L)	$E^{b}_{bind\text{-}Luc}$ (kcal/mol)
Furanone	2,2-Dimethyl-3(2H)-furanone	22D3F	35298-48-7	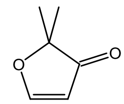	112.13	$(6.76 \pm 0.99) \times 10^{-4}$	−17.37
Furanone	2(5H)-Furanone	2F	497-23-4	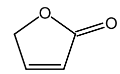	84.07	$(4.47 \pm 0.96) \times 10^{-3}$	−15.88
Furanone	2-Methyltetrahydro-3-furanone	2M3F	3188-00-9	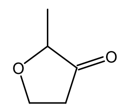	100.12	$(1.86 \pm 0.25) \times 10^{-3}$	−17.08
Furanone	Benzofuran-3(2H)-one	B3O	7169-34-8	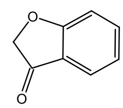	134.13	$(2.95 \pm 0.36) \times 10^{-3}$	−15.47
Furanone	(S)-(−)-5-Hydroxymethyl-2(5H)-furanone	S5H2F	78508-96-0	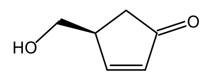	114.10	$(4.90 \pm 0.73) \times 10^{-3}$	−19.63
Furanone	γ-Valerolactone	γV	108-29-2	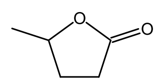	100.12	$(3.55 \pm 0.47) \times 10^{-3}$	−19.70
Pyrrole	1-Pyrrolidino-1-cyclohexene	1P1C	1125-99-1	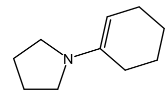	151.25	$(2.88 \pm 0.60) \times 10^{-4}$	−20.12
Pyrrole	(R)-3-Pyrrolidinol	R3P	2799-21-5	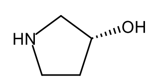	87.12	$(8.13 \pm 1.12) \times 10^{-4}$	−19.08
Pyrrole	(S)-(+)-2-Pyrrolidinemethanol	S2P	23356-96-9	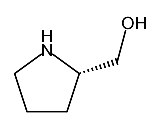	101.15	$(1.10 \pm 0.26) \times 10^{-3}$	−18.64
Pyrrolidone	2-Pyrrolidone-5-carboxylic acid	2P5CA	149-87-1	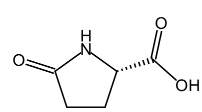	129.11	$(7.24 \pm 1.27) \times 10^{-4}$	−20.17
Sulfonamide	Sulfachloropyridazine	SCP	80-32-0	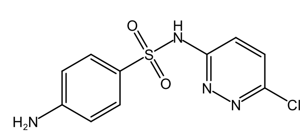	284.72	$(6.46 \pm 0.92) \times 10^{-5}$	−27.92
Sulfonamide	Sulfisoxazole	SIX	127-69-5	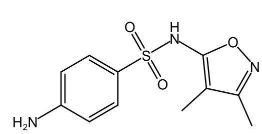	267.30	$(2.51 \pm 0.35) \times 10^{-5}$	−30.43
Sulfonamide	Sulfamethoxazole	SMX	723-46-6	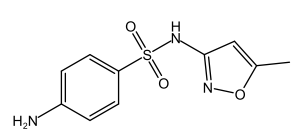	253.28	$(1.10 \pm 0.16) \times 10^{-4}$	−25.85

[a]Mean EC_{50} ± SD represents the mean of the median effective concentration (EC_{50}) for test chemical and the corresponding standard deviation (SD) of five replicate experiments.
[b]The lowest CDOCKER interaction energy between test chemical and luciferase.

2.3. Molecular docking

The bioluminescence of *A. fischeri* is derived from the bioluminescent reaction that catalyzed by luciferase (Luc) (Tian et al., 2022):

$$FMNH_2 + O_2 + RCHO \xrightarrow{\text{Luciferase}} FMN + RCOOH + H_2O + h\nu \quad (2)$$

where Luc binds $FMNH_2$ followed by molecular oxygen and RCHO to form an excited-state complex, which then falls into its ground-state and decomposes into Luc, FMN, RCOOH, water, and redundant energy released as light (490 nm). Therefore, the Luc enzyme was set as the possible target protein for test chemicals in this study. The crystal structure of receptor protein Luc (PDB ID: 3FGC) in *A. fischeri* was downloaded from the RCSB Protein Data Bank (https://www.rcsb.org/). The structures of QSIs and SAs were acquired from Chemical Book (https://www.chemicalbook.com/). The docking simulation was conducted through Discovery Studio 3.1 (DS, Accelrys Software, San Diego, CA, USA) using the CDOCKER protocol with default parameters. The lowest CDOCKER interaction energy ($E_{\text{bind-Luc}}$) between Luc and each chemical was obtained to exhibit their binding affinity that corresponded to the most stable conformation (Gupta et al., 2021; Pan et al., 2021).

2.4. QSAR model development

QSAR models were developed for the EC_{50} values of single chemicals and binary mixtures using univariate and multiple linear regressions in SPSS 19.0 (SPSS Inc. Chicago, IL, USA). The obtained $E_{bind\text{-Luc}}$ was set as the structural descriptor for each chemical. With regard to regression-based QSAR models, the statistical quality of the fitted equations was evaluated using the correlation coefficient (R^2), significant level (P), Fischer F-ratio (F), and root mean standard error (RMSE). Meanwhile, internal and external validations were conducted to estimate the predictive capability and the goodness of fitness of QSAR models. The cross-validation was used for internal validation via leave-one-out (LOO) method and the corresponding metrics Q^2_{loo} was calculated by the following equation (Sun et al., 2019; Wylie and Korchevskiy, 2022):

$$Q^2_{loo} = 1 - \frac{\sum (y_i - \overline{y}_i)^2}{\sum (y_i - y_{mean})^2} \quad (3)$$

where y_i and $\overline{y}_i$ refer to the actual and predicted values of dependent variables in the training sets, respectively; y_{mean} represents to the average of all dependent variables in the training sets. The statistical parameter Q^2_{F1} was employed for external validation, which was calculated by the following equation (Nandi et al., 2018):

$$Q^2_{F1} = 1 - \frac{\sum \left(Y_i - \overline{Y}_i\right)^2}{\sum (Y_i - y_{mean})^2} \quad (4)$$

where Y_i and $\overline{Y}_i$ are the actual and predicted values of dependent variables in the test sets, respectively.

2.5. Applicability domain analysis

According to the OECD principle 3 "a defined domain of applicability", the applicability domain (AD) was considered to define the scope and limitations of the developed QSAR models. The AD of a QSAR model is defined by the corresponding modeling descriptors, which indicates a definite chemical space of the training data (Chatterjee and Roy, 2021). Here, the structural AD of the developed QSAR models was assessed based on the leverage approach and Williams plot (Cao et al., 2020; Peng and Picchioni, 2020). First, the Hat Matrix (H) was defined as:

$$H = X(X^T X)^{-1} X^T \quad (5)$$

where X denoted the molecular descriptors. Thus, the leverage value was then obtained. Second, the structural boundary line h^* value was calculated by:

$$h^* = \frac{3(p + 1)}{n} \quad (6)$$

where p presented the number of modeling descriptors, and n was the number of training compounds. Third, the prediction outlier was identified via the standardized residual method, and the corresponding δ value was calculated from:

$$\delta = \frac{y_{obs} - y_{pred}}{\sqrt{\sum \left(y_{obs} - y_{pred}\right)^2 / (n - p - 1)}} \quad (7)$$

where y_{obs} and y_{pred} respectively referred to the observed and predicted toxicity value. Fourth, the Williams plot that standardized residual versus leverage value was depicted, where AD was displayed with two horizontal lines ($\delta = \pm 3$) and one vertical line (h^* value). When chemicals were within the AD, the corresponding predictions were considered to be reliable and credible.

2.6. Joint toxic action judgment

Toxic unit (TU) was applied to characterize the combined toxicity of QSIs and SAs (Shen et al., 2021; Zhu et al., 2020):

$$TU = \frac{c_{QSI}}{EC_{50(QSI)}} + \frac{c_{SA}}{EC_{50(SA)}} \quad (8)$$

where c_{QSI} and c_{SA} respectively denoted the concentrations of QSI and SA in the binary mixture that provoked the median inhibition on the bioluminescence; $EC_{50(QSI)}$ and $EC_{50(SA)}$ were the EC_{50} values for single QSI and SA, respectively. The joint toxic action was judged: TU < 0.8 indicated the synergistic effect between QSI and SA; 0.8 ≤ TU ≤ 1.2 demonstrated that QSI and SA possessed the additive effect; and 1.2 < TU showed that the joint toxic action between QSI and SA was antagonism. For synergistic effect (TU < 0.8), the smaller the TU value was, the stronger the synergism was. For antagonistic effect (1.2 < TU), the larger the TU value was, the stronger the antagonism was. In this study, the heatmap that corresponded to the TU value was delineated to reflect the joint toxic action between QSI and SA in all binary mixtures. The synergistic and antagonistic effects were displayed in contrasting colors, and the additive effect was expressed in white.

3. Results and discussion

3.1. Acute toxicity of single QSIs and SAs

It was found that all test QSIs and SAs inhibited the bioluminescence of *A. fischeri* in 15 min exposure, and the dose-responses all exhibited S-shape (**Fig. S1**). Table 1 and Fig. 1**A** respectively show the EC_{50} and $-\log EC_{50}$ values for the acute toxicity of QSIs and SAs. The $-\log EC_{50}$ values for test chemicals ranged from 2.31 to 4.60, and the corresponding order was as follows: SIX > SCP > SMX > 1P1C > 22D3F > 2P5CA > R3P > S2P > 2M3F > B3O > γV > 2F > S5H2F. It was obvious that SAs induced greater toxic effects than QSIs. Furthermore, 1P1C and 22D3F were respectively the most toxic chemicals among test pyrroles and furanones.

The J-shaped hormetic dose-responses of QSIs and SAs to *A. fischeri* bioluminescence could be observed in chronic toxicity tests, where the exposure time was usually set at 24 h (Sun et al., 2020; You et al., 2016). As reported in previous studies, the maximum stimulation of QSIs and SAs could be larger than 100 % and 50 %, respectively (Sun et al., 2020; You et al., 2016). Comparing the acute (15 min) and chronic (24 h) toxicity values, it could be found that the acute toxicity of each QSI was

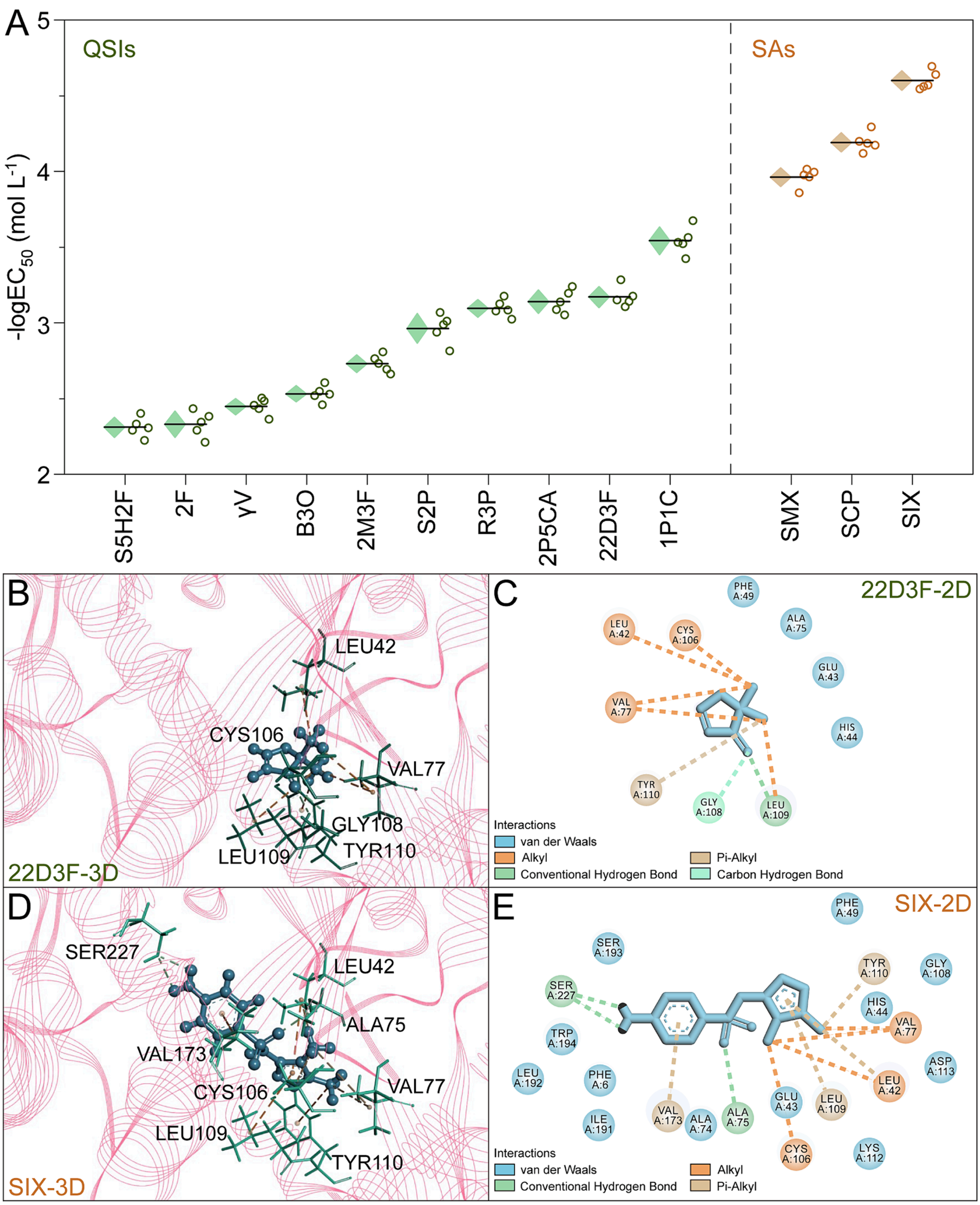

Fig. 1. (A) The acute toxicity of single QSIs and SAs to *A. fischeri* bioluminescence. The mean value (the black line) and the standard deviation (the upper and lower limits of the diamond) of $-\log EC_{50}$ for each chemical were calculated from 5 replicates; (B and C) the optimal docked position of 22D3F with Luc (3D) and the interactions with surrounding amino acids (2D); and (D and E) the optimal docked position of SIX with Luc (3D) and the interactions with surrounding amino acids (2D). Abbreviations: QSIs, quorum sensing inhibitors; SAs, sulfonamides; *A. fischeri*, *Aliivibrio fischeri*; EC_{50}, median effective concentration; Luc, luciferase; 22D3F, 2,2-Dimethyl-3(2H)-furanone; 2F, 2(5H)-Furanone; 2M3F, 2-Methyltetrahydro-3-furanone; B3O, Benzofuran-3(2H)-one; S5H2F, (S)-(−)-5-Hydroxymethyl-2(5H)-furanone; γV, γ-Valerolactone; 1P1C, 1-Pyrrolidino-1-cyclohexene; R3P, (R)-3-Pyrrolidinol; S2P, (S)-(+)-2-Pyrrolidinemethanol; 2P5CA, 2-Pyrrolidone-5-carboxylic acid; SCP, sulfachloropyridazine; SIX, sulfisoxazole; SMX, sulfamethoxazole.

usually larger than its chronic toxicity, while the SA's acute toxicity was less than its chronic toxicity (Sun et al., 2020; You et al., 2016). For example, $-\log EC_{50}$ values for B3O in acute and chronic toxicity were 2.53 and 1.86, respectively; EC_{50} for SIX were respectively 2.51×10^{-5} mol/L and 1.32×10^{-5} mol/L in 15 min and 24 h exposure. In chronic toxicity test, modified-marine photobacterium broth was added into the culture system to provide sufficient nutrients for the growth and metabolism of *A. fischeri*. The continuous proliferation of *A. fischeri* in 24 h activated the QS system, and thus QSIs and SAs could act on the QS signaling pathways to stimulate the bioluminescence (Sun et al., 2018). Because there was no additional nutrition constituent in the acute toxicity test, the growth of *A. fischeri* was limited under 15 min exposure. In these circumstances, QSIs and SAs could not stimulate the bioluminescence by provoking the QS system and inhibit the bioluminescence by binding to their target proteins. Hence, significant differences were observed in the acute and chronic toxicity of QSIs and SAs, especially in the manifestation of hormesis.

Previous studies have suggested that exogenous chemicals probably act on the Luc enzyme to trigger acute toxic effects on *A. fischeri* bioluminescence (Fan et al., 2020). Using the active site of Luc that catalyzed the bioluminescent reaction as the active pocket, the molecular docking was conducted between Luc and each chemical. 22D3F and SIX were respectively selected as the representatives for QSIs and SAs. The optimal docked positions of these two chemicals with Luc (3D) and their interactions with surrounding amino acids (2D) are depicted in Fig. 1**B-1E**. **Fig. S2** displays the docking results of rest chemicals with Luc. It could be observed that test chemicals bind tightly to Luc, and van der Waals force, hydrogen bond, and hydrophobic bond were the main interaction types (**Table S3**). Furthermore, the bound amino acids in the active pocket, such as CYS106, LEU42, and LEU109, have been clarified the pivotal role in exhibiting the catalytic activity of Luc in previous studies (Giuliani et al., 2021; Kim et al., 2018; Tinikul and Chaiyen, 2016; Yao et al., 2023). Hence, it could be speculated that QSIs and SAs might act on the active site of Luc to induce acute toxicity to *A. fischeri* bioluminescence.

E_{bind} is a key descriptor to reflect the strength of interaction between biomacromolecule and ligand (Wang et al., 2018b). In general, the smaller the E_{bind} is, the stronger the interaction is. Table 1 lists the $E_{\text{bind-Luc}}$ values between test chemicals and Luc. While the $E_{\text{bind-Luc}}$ values for QSIs ranged from −20.17 to −15.47 kcal/mol, the $E_{\text{bind-Luc}}$ values for SCP, SIX, and SMX were respectively −27.92, −30.43, and −25.85 kcal/mol. The smaller $E_{\text{bind-Luc}}$ values for SAs might result from the greater number of bonds, indicating the stronger interactions between SAs and Luc. These docking results might account for the larger acute toxicity of SAs than QSIs.

3.2. QSAR model for the acute toxicity of single chemicals

To further validate the vital role of acting on Luc in triggering acute toxicity to *A. fischeri* bioluminescence, QSAR model was constructed for the acute toxicity of test chemicals using $E_{\text{bind-Luc}}$ as the structural descriptor:

$$-\log EC_{50} = 0.330 - 0.140 \times E_{\text{bind-Luc}} \quad (9)$$

$n = 10$, $R^2 = 0.769$, $\text{RMSE} = 0.347$, $F = 30.880$, $P < 0.001$, $Q^2_{loo} = 0.737$, $\text{RMSE}_{loo} = 0.351$, $Q^2_{F1} = 0.768$, $\text{RMSEP} = 0.202$.

As shown in Equation (9), the R^2 of QSAR model was 0.774 (>0.60), indicating high goodness-of-fit of the model (Xiao et al., 2015). Furthermore, Q^2_{loo} and Q^2_{F1} values were greater than 0.50, which suggested that the model has good robustness and predictive ability (Golbraikh and Tropsha, 2002; Lavado et al., 2022). Fig. 2**A** depicts the scatter plots of the experimental $-\log EC_{50}$ value versus the predicted $-\log EC_{50}$ value of the QSAR model. All scatters distributed near the trend line, suggesting the good predictive ability of the model. Moreover, the AD of QSAR model was characterized by Williams plot (Fig. 2**B**). Every absolute standard residual for the training and test sets was lower than 3, demonstrating that there were no outliers. The leverage values for both the training and test sets were all smaller than the warning value ($h^* = 2.0$), indicating the robust representativeness of the training set (Cheng et al., 2022). Hence, the constructed QSAR model for the acute toxicity of test chemicals met the requirements for a QSAR model's regulator application according to OECD guidelines. These results further verified that Luc was the target protein of the test chemicals when resulting in the acute inhibition on *A. fischeri* bioluminescence.

3.3. Acute toxicity of binary mixtures for QSIs and SAs at equitoxic ratio and its QSAR model

Given the co-existence of QSIs and SAs in the environment, the acute toxic effects of their mixtures were also determined. The binary mixtures of QSIs and SAs were obtained based on the equitoxic ratio of EC_{50} for each chemical, which was the common mixing method in combined toxicity test. **Fig. S3** depict that the binary mixtures only inhibit the bioluminescence. Table 2 and Fig. 3**A** respectively display the $EC_{50(\text{mix})}$ and $-\log EC_{50(\text{mix})}$ values for the acute toxicity of QSI-SA (1:1) mixtures. It was observed that γV-SAs and S5H2F-SAs mixtures triggered the lowest $-\log EC_{50(\text{mix})}$ values, while the binary mixtures of B3O and SAs could lead to the largest toxic effects on *A. fischeri* bioluminescence. In the 16 groups of binary mixtures, B3O-SIX and γV-SIX were the most and least toxic mixtures, respectively. It could be found from previous studies that the chronic toxicity (24 h) for binary mixtures of QSIs and SAs exhibited hormetic phenomenon, where the maximum stimulation was generally larger than 100 % (Sun et al., 2020; You et al., 2016). Furthermore, the acute toxicity for each QSI-SA mixture was usually larger than its chronic toxicity (Sun et al., 2020; You et al., 2016). For instance, EC_{50} values for the acute and chronic toxicity of B3O-SIX were 7.20×10^{-5} mol/L and 1.70×10^{-3} mol/L, respectively.

The prediction for the combined toxicity of chemical mixtures is a challenging task in environmental risk assessment (Kumari and Kumar, 2020; Landi et al., 2022). Previous studies have usually optimized the

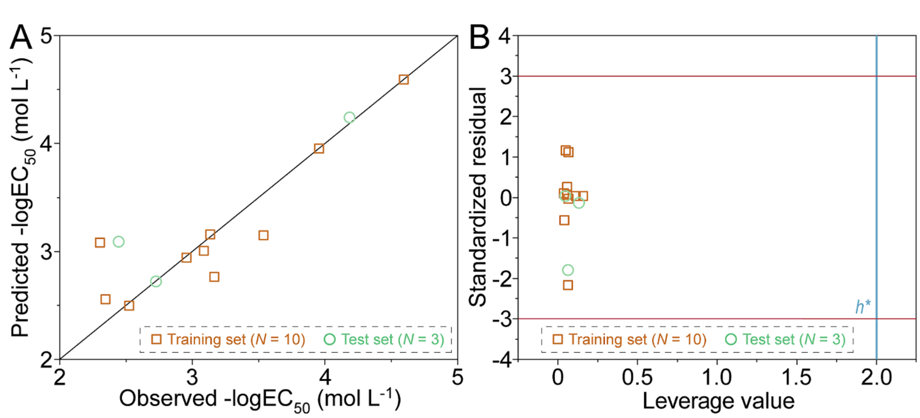

Fig. 2. (A) The predicted $-\log EC_{50}$ values of single chemicals from the QSAR model (Equation (9)) versus the observed $-\log EC_{50}$ values; and (B) the Williams plot indicating the applicability domain of the QSAR model (Equation (9)). Abbreviations: EC_{50}, median effective concentration; QSAR, quantitative structure–activity relationship.

Table 2
The acute toxicity for the binary mixtures of QSIs and SAs to *A. fischeri* bioluminescence and the parameters in corresponding QSAR models.

Binary mixture (QSI:SA)	Toxicity ratio ($EC_{50(QSI)}$:$EC_{50(SA)}$)	Mean $EC_{50(mix)}$ ± SD[a] (mol/L)	p_{QSI}[b]	p_{SA}[c]	c_{QSI}[d] (mol/L)	c_{SA}[e] (mol/L)	$p_{QSI} \times E^{QSI}_{bind\text{-}Luc}$[f] (kcal/mol)	$p_{SA} \times E^{SA}_{bind\text{-}Luc}$[g] (kcal/mol)
22D3F:SIX	1:1	$(1.38 \pm 0.11) \times 10^{-4}$	0.964	0.036	1.33×10^{-4}	4.94×10^{-6}	−16.743	−1.090
22D3F:SMX	1:1	$(3.02 \pm 0.19) \times 10^{-4}$	0.860	0.140	2.60×10^{-4}	4.21×10^{-5}	−14.942	−3.608
2F:SIX	1:1	$(1.35 \pm 0.10) \times 10^{-4}$	0.994	0.006	1.34×10^{-4}	7.54×10^{-7}	−15.788	−0.170
2F:SMX	1:1	$(1.32 \pm 0.08) \times 10^{-4}$	0.976	0.024	1.29×10^{-4}	3.16×10^{-6}	−15.497	−0.619
S5H2F:SIX	1:1	$(3.47 \pm 0.29) \times 10^{-3}$	0.995	0.005	3.45×10^{-3}	1.77×10^{-5}	−19.530	−0.155
S5H2F:SMX	1:1	$(1.86 \pm 0.13) \times 10^{-3}$	0.978	0.022	1.82×10^{-3}	4.08×10^{-5}	−19.201	−0.566
γV:SMX	1:1	$(2.24 \pm 0.16) \times 10^{-3}$	0.970	0.030	2.17×10^{-3}	6.71×10^{-5}	−19.106	−0.775
1P1C:SMX	1:1	$(3.72 \pm 0.34) \times 10^{-4}$	0.725	0.275	2.69×10^{-4}	1.02×10^{-4}	−14.580	−7.122
R3P:SIX	1:1	$(5.89 \pm 0.30) \times 10^{-4}$	0.970	0.030	5.71×10^{-4}	1.77×10^{-5}	−18.507	−0.912
S2P:SIX	1:1	$(8.32 \pm 0.30) \times 10^{-4}$	0.978	0.022	8.13×10^{-4}	1.86×10^{-5}	−18.221	−0.682
2P5CA:SMX	1:1	$(9.12 \pm 0.45) \times 10^{-4}$	0.869	0.131	7.92×10^{-4}	1.20×10^{-4}	−17.522	−3.399
2M3F:SIX	1:10	$(3.02 \pm 0.36) \times 10^{-4}$	0.881	0.119	2.66×10^{-4}	3.59×10^{-5}	−15.048	−3.617
	1:5	$(2.57 \pm 0.22) \times 10^{-4}$	0.937	0.063	2.41×10^{-4}	1.62×10^{-5}	−15.998	−1.923
	1:1	$(2.45 \pm 0.33) \times 10^{-4}$	0.987	0.013	2.42×10^{-4}	3.27×10^{-6}	−16.850	−0.405
	1:0.2	$(2.20 \pm 0.29) \times 10^{-4}$	0.997	0.003	2.18×10^{-4}	5.89×10^{-7}	−17.032	−0.082
	1:0.1	$(1.74 \pm 0.15) \times 10^{-4}$	0.999	0.001	1.74×10^{-4}	2.34×10^{-7}	−17.054	−0.041
2M3F:SMX	1:10	$(2.09 \pm 0.12) \times 10^{-4}$	0.629	0.371	1.31×10^{-4}	7.74×10^{-5}	−10.748	−9.582
	1:5	$(1.95 \pm 0.14) \times 10^{-4}$	0.773	0.227	1.51×10^{-4}	4.44×10^{-5}	−13.193	−5.881
	1:1	$(1.91 \pm 0.15) \times 10^{-4}$	0.944	0.056	1.80×10^{-4}	1.06×10^{-5}	−16.128	−1.438
	1:0.2	$(1.86 \pm 0.14) \times 10^{-4}$	0.988	0.012	1.84×10^{-4}	2.17×10^{-6}	−16.879	−0.301
	1:0.1	$(1.78 \pm 0.13) \times 10^{-4}$	0.994	0.006	1.77×10^{-4}	1.04×10^{-6}	−16.978	−0.151
B3O:SCP	1:10	$(1.91 \pm 0.17) \times 10^{-4}$	0.820	0.180	1.56×10^{-4}	3.42×10^{-5}	−12.690	−5.012
	1:5	$(1.32 \pm 0.09) \times 10^{-4}$	0.901	0.099	1.19×10^{-4}	1.30×10^{-5}	−13.941	−2.753
	1:1	$(7.79 \pm 0.66) \times 10^{-5}$	0.979	0.021	7.60×10^{-5}	1.66×10^{-6}	−15.135	−0.598
	1:0.2	$(7.43 \pm 0.56) \times 10^{-5}$	0.996	0.004	7.38×10^{-5}	3.23×10^{-7}	−15.398	−0.122
	1:0.1	$(6.78 \pm 0.55) \times 10^{-5}$	0.998	0.002	6.75×10^{-5}	1.48×10^{-7}	−15.432	−0.061
B3O:SIX	1:10	$(1.10 \pm 0.07) \times 10^{-4}$	0.922	0.078	1.01×10^{-4}	8.60×10^{-6}	−14.253	−2.387
	1:5	$(9.80 \pm 0.83) \times 10^{-5}$	0.959	0.041	9.37×10^{-5}	3.99×10^{-6}	−14.834	−1.242
	1:1	$(7.26 \pm 0.57) \times 10^{-5}$	0.992	0.008	7.18×10^{-5}	6.11×10^{-7}	−15.335	−0.257
	1:0.2	$(6.95 \pm 0.72) \times 10^{-5}$	0.998	0.002	6.91×10^{-5}	1.18×10^{-7}	−15.440	−0.052
	1:0.1	$(6.19 \pm 0.55) \times 10^{-5}$	0.999	0.001	6.16×10^{-5}	5.24×10^{-8}	−15.453	−0.026
γV:SIX	1:10	$(5.13 \pm 0.40) \times 10^{-3}$	0.934	0.066	4.79×10^{-3}	3.39×10^{-4}	−18.394	−2.012
	1:5	$(4.79 \pm 0.46) \times 10^{-3}$	0.966	0.034	4.62×10^{-3}	1.64×10^{-4}	−19.023	−1.040
	1:1	$(4.47 \pm 0.50) \times 10^{-3}$	0.993	0.007	4.44×10^{-3}	3.14×10^{-5}	−19.558	−0.214
	1:0.2	$(4.17 \pm 0.49) \times 10^{-3}$	0.999	0.001	4.16×10^{-3}	5.89×10^{-6}	−19.668	−0.043
	1:0.1	$(4.07 \pm 0.46) \times 10^{-3}$	0.999	0.001	4.07×10^{-3}	2.88×10^{-6}	−19.682	−0.022

[a]The Mean $EC_{50(mix)}$ ± SD represent the mean of the median effective concentration ($EC_{50(mix)}$) for binary mixtures and the corresponding standard deviation (SD) of five replicate experiments.
[b]The apparent concentration proportion of QSI in each binary mixture.
[c]The apparent concentration proportion of SA in each binary mixture.
[d]The QSI concentration in each binary mixture that provoked the median inhibition.
[e]The SA concentration in each binary mixture that provoked the median inhibition.
[f]The structural descriptor of the QSI in corresponding QSAR models of the binary mixtures, and the $E^{QSI}_{bind\text{-}Luc}$ represent the lowest CDOCKER interaction energy between QSI and luciferase.
[g]The structural descriptor of the SA in corresponding QSAR models of the binary mixtures, and the $E^{SA}_{bind\text{-}Luc}$ represent the lowest CDOCKER interaction energy between QSI and luciferase.

used structural descriptor via some parameters to better reflect the contribution of component to the joint effects, which could markedly increase the forecast accuracy of the QSAR model for combined toxicity (Algamal et al., 2020; Szucs et al., 2023). For example, interaction energy between the component i and its target protein (E_{bind}) could be multiplied by the apparent concentration proportion of component i in the mixture (p_i) to reflect the contribution of the component for combined toxicity (Zou et al., 2012; Wang et al., 2018b). In this study, the constructed QSAR model for acute toxicity of single QSIs and SAs in Equation (9) indicated the reasonability of $E_{bind\text{-}Luc}$ as the structural descriptor. Thus, the QSAR model for combined toxicity of QSIs and SAs at equitoxic ratio was developed using $E_{bind\text{-}Luc}$ value and p value for each chemical:

$$-\log EC_{50(mix)} = \quad \times p_{QSI} \times E^{QSI}_{bind-Luc} + \times p_{SA} \times E^{SA}_{bind-Luc} \tag{10}$$

$n = 12$, $R^2 = 0.893$, RMSE $= 0.179$, $F = 46.763$, $P < 0.001$, $Q^2_{loo} = 0.859$, $RMSE_{loo} = 0.197$, $Q^2_{F1} = 0.888$, RMSEP $= 0.132$.

Table 2 lists the p value for QSI and SA in each mixture at equitoxic ratio as well as $p \times E_{bind\text{-}Luc}$ for each component. The statistical results of Equation (10) indicated that the model possessed goodness-of-fit ($R^2 >$ 0.60), good robustness and predictive ability ($Q^2_{loo} > 0.50$ and $Q^2_{F1} > 0.50$). Moreover, the scatters that the experimental $-\log EC_{50(mix)}$ value versus the predicted $-\log EC_{50(mix)}$ value of QSAR model distribute near the trend line in Fig. 3**B**. According to the AD of the model (Fig. 3**C**), there were no outlier data for the absolute values of standardized residuals, and none of the tested mixtures was particularly influential in the model space. These findings also manifested the good predictive ability for the model and the good representativeness for the data set. As shown in Table 2, QSIs had the larger apparent concentration proportions (p_{QSI}: from 0.629 to 0.999) than SAs (p_{SA}: from 0.001 to 0.371) in binary mixtures. In combination with the coefficients for QSI (0.329) and SA (0.128) from the QSAR model, it could be obtained that QSIs were more involved in the interaction with Luc than SAs. In addition, $p_{QSI} \times E^{QSI}_{bind\text{-}Luc}$ values (from −19.682 to −10.748) were significantly smaller than $p_{SA} \times E^{SA}_{bind\text{-}Luc}$ values (from −9.582 to −0.022). Hence, QSIs possibly contributed more to the acute toxicity of binary mixtures for QSIs and SAs at equitoxic ratio.

3.4. Influence of QSI proportion on the acute toxicity of QSI-SA mixtures

When QSIs and SAs enter the environment, they may co-exist at

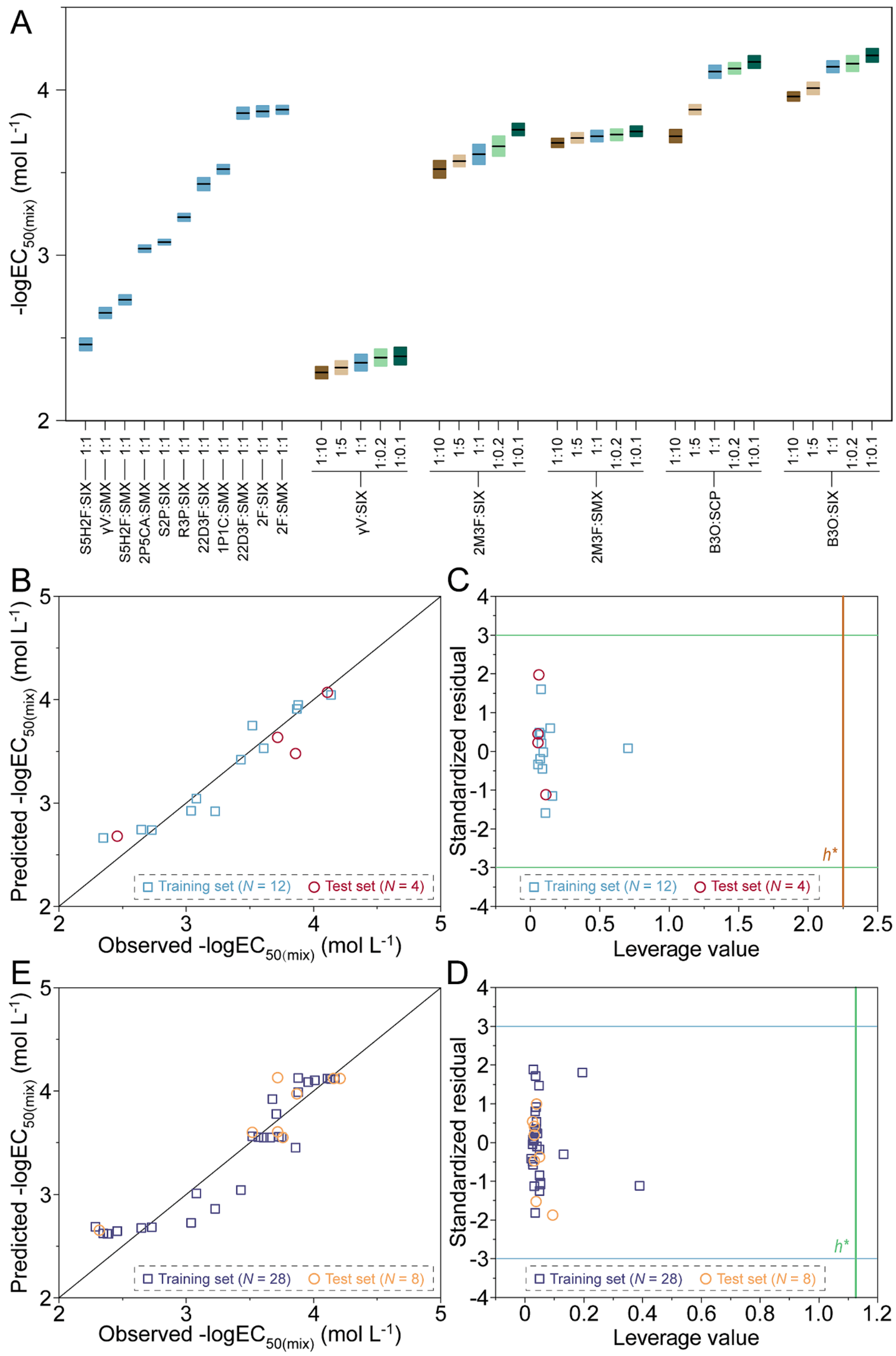

Fig. 3. (A) The acute toxicity of binary mixtures for QSIs and SAs to *A. fischeri* bioluminescence. The mean value (the black line) and the standard deviation (the upper and lower limits of the box) of $-\log EC_{50(mix)}$ for each mixture were calculated from 5 replicates; (B) the predicted $-\log EC_{50(mix)}$ values of binary mixtures from the QSAR model (Equation (10)) versus the observed $-\log EC_{50(mix)}$ values; (C) the Williams plot indicating the applicability domain of the QSAR model (Equation (10)); (D) the predicted $-\log EC_{50(mix)}$ values of all binary mixtures from the QSAR model (Equation (11)) versus the observed $-\log EC_{50(mix)}$ values; and (E) the Williams plot indicating the applicability domain of the QSAR model (Equation (11)).1:1, 1:10, 1:5, 1:0.2, and 1:0.1 indicate the ratios of $EC_{50(QSI)}$ and $EC_{50(SA)}$, which are used to design the binary mixtures. Abbreviations: QSIs, quorum sensing inhibitors; SAs, sulfonamides; *A. fischeri*, *Aliivibrio fischeri*; EC_{50}, median effective concentration; QSAR, quantitative structure–activity relationship; 22D3F, 2,2-Dimethyl-3(2H)-furanone; 2F, 2(5H)-Furanone; 2M3F, 2-Methyltetrahydro-3-furanone; B3O, Benzofuran-3(2H)-one; S5H2F, (S)-(−)-5-Hydroxymethyl-2(5H)-furanone; γV, γ-Valerolactone; 1P1C, 1-Pyrrolidino-1-cyclohexene; R3P, (R)-3-Pyrrolidinol; S2P, (S)-(+)-2-Pyrrolidinemethanol; 2P5CA, 2-Pyrrolidone-5-carboxylic acid; SCP, sulfachloropyridazine; SIX, sulfisoxazole; SMX, sulfamethoxazole.

various ratios. Thus, it is also necessary to evaluate the influence of component concentration on the acute toxicity of QSI-SA mixtures. Here, 2M3F-SIX, 2M3F-SMX, B3O-SCP, B3O-SIX, and γV-SIX were selected as the representative pairs, and their binary mixtures were designed via setting the ratios of $EC_{50(QSI)}$ to $EC_{50(SA)}$ at 1:10, 1:5, 1:0.2, and 1:0.1. As displayed in Fig. 3**A** and Table 2, with the increase of the proportion for QSI component, the $-\log EC_{50(mix)}$ values (or $EC_{50(mix)}$ values) were enlarged (or decreased) for 2M3F-SIX, 2M3F-SMX, B3O-SCP, B3O-SIX, and γV-SIX mixtures. For instance, the $EC_{50(mix)}$ of B3O-SCP (1:10) was 1.91×10^{-4} mol/L, which was reduced to 6.78×10^{-5} mol/L when the proportion of B3O increased to 99.8 % in the mixture. These results manifested that the increase of QSI proportion could enhance the acute toxicity of QSI-SA mixtures, which supported the above speculation for the more contribution of QSIs in the combined toxicity.

3.5. QSAR model for the acute toxicity of QSI-SA mixtures

Could we forecast the acute toxicity of the binary mixtures for QSIs and SAs at different ratios? This issue is significant for comprehensively assessing the environmental risk of QSI-SA mixtures. The practicable QSAR model in Equation (10) used the component proportion (p) to describe the feature for the mixed exposure of QSIs and SAs, which realized the accurate prediction for combined toxicity of QSI-SA mixtures at equitoxic ratios. Thus, the p parameter could also reflect the component information in the binary mixtures of QSIs and SAs at different ratios. Table 2 lists the p value for each component in 2M3F-SIX, 2M3F-SMX, B3O-SCP, B3O-SIX, and γV-SIX mixtures where the ratios of $EC_{50(QSI)}$ to $EC_{50(SA)}$ were respectively 1:10, 1:5, 1:0.2, and 1:0.1. Here, the QSAR model that taken the acute toxicity of all binary mixtures of QSIs and SAs at equitoxic and non-equitoxic ratios into account was constructed using p and $E_{\text{bind-Luc}}$ parameters:

$$-\log EC_{50(\text{mix})} = 9.627 + 0.356 \times p_{\text{QSI}} \times E_{\text{bind - Luc}}^{\text{QSI}} + 0.196 \times p_{\text{SA}} \times E_{\text{bind - Luc}}^{\text{SA}} \tag{11}$$

$n = 28$, $R^2 = 0.880$, RMSE $= 0.217$, $F = 100.046$, $P < 0.001$, $Q^2_{loo} = 0.846$, $\text{RMSE}_{loo} = 0.242$, $Q^2_{F1} = 0.878$, RMSEP $= 0.113$.

$R^2 > 0.60$, $Q^2_{loo} > 0.50$, and $Q^2_{F1} > 0.50$ suggested this QSAR model had goodness-of-fit, good robustness, and predictive ability. Fig. 3**D** exhibits a satisfactory agreement between the experimental and predicted $-\log EC_{50(\text{mix})}$ values, which also demonstrates the good predictive ability of QSAR model. Furthermore, Fig. 3**E** indicates that the training and test sets were all within the AD of the QSAR model, indicating that the prediction results were reliable and credible. Compared with the model in Equation (10), this QSAR model included the combined toxicity results of QSIs and SAs at both equitoxic and non-equitoxic ratios, which possessed a wider application in environmental risk assessment of QSI-SA mixtures. The larger coefficient and $p \times E_{\text{bind-Luc}}$ values for QSI indicated that more QSIs bind with Luc than SA, and QSI was always the major contributor in the combined toxicity of QSIs and SAs even though the QSI proportion varied. In addition, the favorable QSAR model in Equation (11) illustrated that as long as the proportion information of component and the corresponding $E_{\text{bind-Luc}}$ value were provided, the acute toxicity for QSI-SA mixtures could be effectively predicted.

3.6. Joint toxic actions of QSIs and SAs in acute toxicity

Besides the toxicity value, the joint toxic action is also a crucial indicator in the environmental risk assessment of the mixture (Tang et al., 2022). The observed TU values for the binary mixture of QSIs and SAs are listed in **Table S4**. The heatmap that corresponded to the TU value is displayed in Fig. 4 to visualize the variation of joint toxic action. In 36 groups of binary mixtures, 23 mixtures exhibited synergistic effects, 12 mixtures possessed antagonistic effects, and only 2M3F-SIX mixture ($EC_{50(2M3F)}$:$EC_{50(SIX)}$ = 1:5) had additive effect (TU = 0.81). While B3O-SIX mixture ($EC_{50(B3O)}$:$EC_{50(SIX)}$ = 1:0.1) triggered the maximum synergism (TU = 0.02), the maximum antagonism (TU = 14.85) was observed for γV-SIX mixture ($EC_{50(\gamma V)}$:$EC_{50(SIX)}$ = 1:10). Furthermore, it could be obtained that the TU values decreased with the increase of QSI proportion in the mixture. For example, when the ratio of $EC_{50(2M3F)}$ to $EC_{50(SIX)}$ changed from 1:10 to 1:0.1, the TU value for 2M3F-SIX mixture varied from 1.57 to 0.10. It should be noted that 2M3F-SMX, B3O-SCP, and B3O-SIX mixtures all exhibited synergism at all ratios of QSI to SA, and the synergistic effect all enhanced with QSI proportion. However, the joint toxic actions between γV and SIX were antagonism in all mixtures, the intensity of which reduced with the increase of γV proportion. Since the acute toxicity of test chemicals to *A. fischeri* bioluminescence resulted from affecting on the active site of Luc, it could be speculated that the synergistic effect between QSI and SA might originate from their cooperation on inhibiting the catalytic activity of Luc. Moreover, the binding of SA to Luc might prevent the interaction of QSI on the same site in some mixtures, resulting in the antagonism between QSI and SA.

Whether the joint toxic action of the mixture could be judged via the structural descriptor and proportion information for each component? This task will save a lot of manpower and material resources for environmental risk assessment, and provide new insights into the evaluation of joint effects for the mixed pollutants. In this study, the joint toxic action was tried to predict based on the QSAR models for the acute toxicity of QSIs and SAs (Equation (9)) as well as QSI-SA mixtures (Equation (11)). First, the EC_{50} values of single QSIs and SAs were predicted via Equation (9). Using these EC_{50} values, the ratio of QSI to SA in the binary mixture could be determined. Based on the predicted $EC_{50(\text{mix})}$ value for the mixture from Equation (11), the concentrations of QSI and SA in the binary mixtures were calculated. At last, the predicted TU value of the mixture was obtained via Equation (8). **Table S4** lists the calculation results for the above parameters and predicted TU values. As shown in Fig. 5, the predicted joint toxic actions between QSIs and SAs exhibited high consistency with the observed results, although there were differences between the predicted and observed TU values. In the

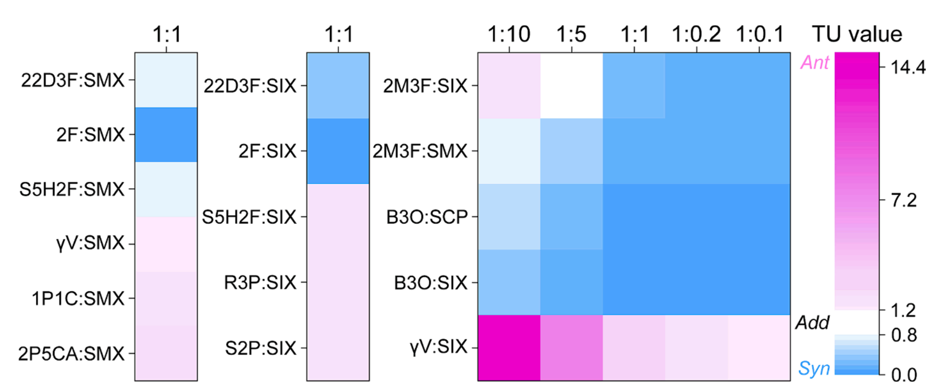

Fig. 4. The heatmaps of TU values for the binary mixtures of QSIs and SAs. TU < 0.8, 0.8 ≤ TU ≤ 1.2, and TU < 1.2 represent synergism (*Syn*), addition (*Add*) and antagonism (*Ant*), respectively. TU value corresponds to each color gradation. 1:1, 1:10, 1:5, 1:0.2, and 1:0.1 indicate the ratios of $EC_{50(QSI)}$ and $EC_{50(SA)}$, which are used to design the binary mixtures. Abbreviations: TU, toxic unit; QSIs, quorum sensing inhibitors; SAs, sulfonamides; EC_{50}, median effective concentration; 22D3F, 2,2-Dimethyl-3(2H)-furanone; 2F, 2(5H)-Furanone; 2M3F, 2-Methyltetrahydro-3-furanone; B3O, Benzofuran-3(2H)-one; S5H2F, (S)-(−)-5-Hydroxymethyl-2(5H)-furanone; γV, γ-Valerolactone; 1P1C, 1-Pyrrolidino-1-cyclohexene; R3P, (R)-3-Pyrrolidinol; S2P, (S)-(+)-2-Pyrrolidinemethanol; 2P5CA, 2-Pyrrolidone-5-carboxylic acid; SCP, sulfachloropyridazine; SIX, sulfisoxazole; SMX, sulfamethoxazole.

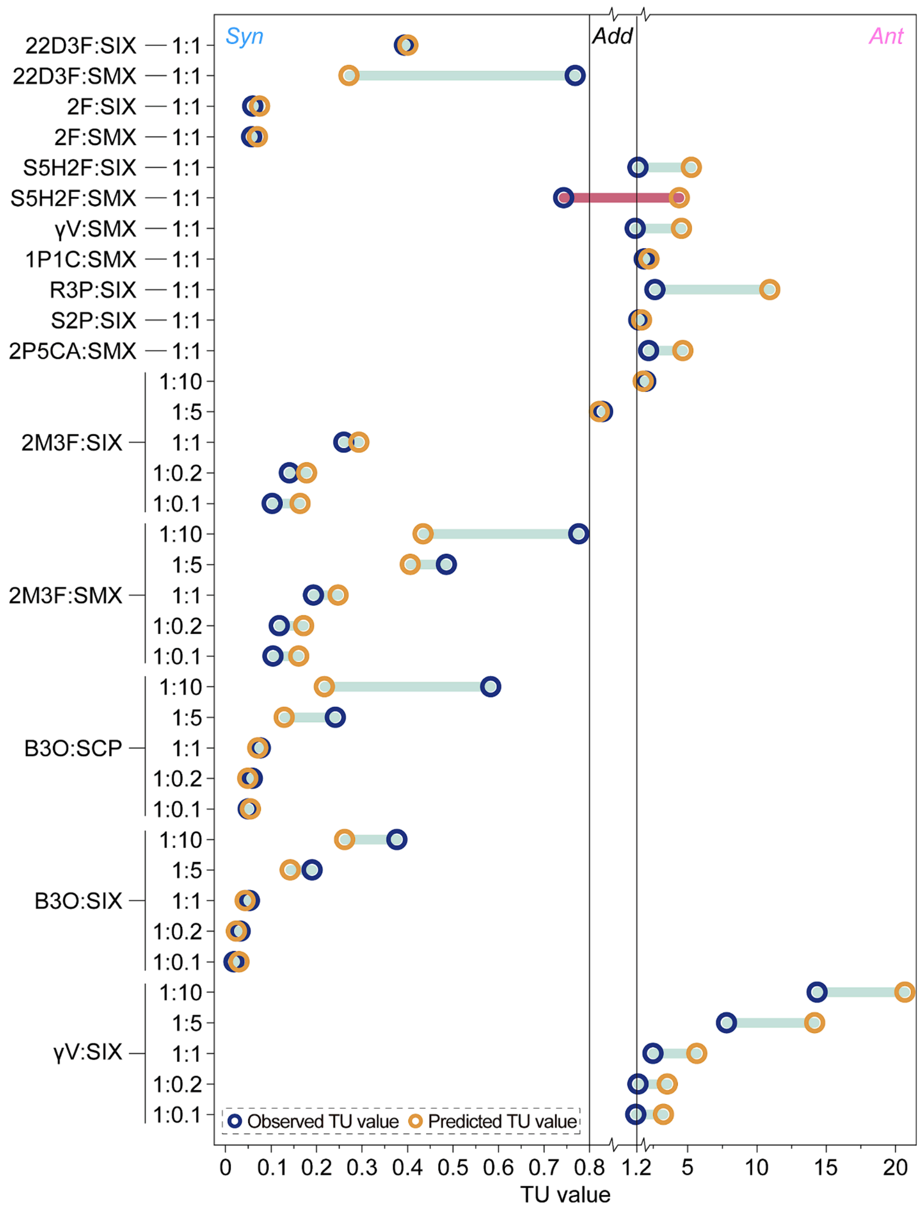

Fig. 5. Dumbbell plot of the differences between the observed and predicted TU values, and the corresponding judgments of joint toxic actions for QSIs and SAs. *Syn*, *Add* and *Ant* represent synergistic, additive, and antagonistic effects, respectively. The green line linking the observed and predicted TU values indicate the same judgment of joint toxic action via the observed and predicted TU values, and the red line indicate the different judgments of joint toxic action via the observed and predicted TU values. Abbreviations: TU, toxic unit; QSIs, quorum sensing inhibitors; SAs, sulfonamides; 22D3F, 2,2-Dimethyl-3(2H)-furanone; 2F, 2(5H)-Furanone; 2M3F, 2-Methyltetrahydro-3-furanone; B3O, Benzofuran-3(2H)-one; S5H2F, (S)-(−)-5-Hydroxymethyl-2(5H)-furanone; γV, γ-Valerolactone; 1P1C, 1-Pyrrolidino-1-cyclohexene; R3P, (R)-3-Pyrrolidinol; S2P, (S)-(+)-2-Pyrrolidinemethanol; 2P5CA, 2-Pyrrolidone-5-carboxylic acid; SCP, sulfachloropyridazine; SIX, sulfisoxazole; SMX, sulfamethoxazole. (For interpretation of the references to color in this figure legend, the reader is referred to the web version of this article.)

test binary mixtures of QSIs and SAs (36 groups), our proposed method could accurately forecast the joint toxic actions of 35 mixtures, only failure for S5H2F-SMX (at equitoxic ratio). These results not only further proved the applicability and accuracy of the constructed QSAR models, but also given a novel approach for exploring the joint effects of mixtures.

4. Conclusion

In this study, the acute toxicity of QSIs, SAs, and their binary mixtures was tested using *A. fischeri* bioluminescence as the endpoint. There was no hormetic phenomenon in 15 min exposure of each chemical and mixture, and all dose–response relationships exhibited S-shape. Although SAs induced greater toxic effects than QSIs in individual exposure, QSIs contributed more to the acute toxicity of QSI-SA mixtures at both equitoxic and non-equitoxic ratios. Furthermore, the increase of QSI proportion in the mixture enhanced the combined toxicity of QSIs and SAs, but decreased the corresponding TU values. The synergism was the main joint toxic action between QSI and SA. Molecular docking results indicated that QSIs and SAs might interacted with Luc to reduce its catalytic activity, thus inducing inhibition on the bioluminescence. Using E_{bind} as the structural descriptor and component proportion as the key parameter, the QSAR models for the acute toxicity of QSIs, SAs, and their mixtures were both developed, which exhibited good robustness and predictive ability. In addition, the joint toxic actions between QSIs and SAs could be successfully forecasted using the constructed QSAR models. This study provides the reference data for the acute toxicity for QSIs and QSI-SA mixtures, and develops the QSAR models for predicting their toxicity value and joint toxic action, which will benefit the environmental risk assessment of QSIs.

CRediT authorship contribution statement

Zhenheng Long: Data curation, Investigation, Formal analysis, Software, Visualization, Writing – original draft. **Jingyi Yao:** Methodology, Visualization. **Minghong Wu:** Supervision, Project administration. **Shu-shen Liu:** Software. **Liang Tang:** Conceptualization, Investigation, Formal analysis, Methodology, Supervision, Writing – review & editing. **Bo Lei:** Validation. **Jiajun Wang:** Formal analysis. **Haoyu Sun:** Conceptualization, Funding acquisition, Investigation, Methodology, Resources, Writing – review & editing.

Declaration of competing interest

The authors declare that they have no known competing financial interests or personal relationships that could have appeared to influence the work reported in this paper.

Data availability

Data will be made available on request.

Acknowledgment

This work was supported by the National Natural Science Foundation of China (42277270, 42107416, and 42377359).

Appendix A. Supplementary data

Supplementary data to this article can be found online at https://doi.org/10.1016/j.crtox.2024.100172.

References

Abbas, M., Adil, M., Ehtisham-ul-Haque, S., Munir, B., Yameen, M., Ghaffar, A., Shar, G. A., Asif Tahir, M., Iqbal, M., 2018. *Vibrio fischeri* bioluminescence inhibition assay for ecotoxicity assessment: A review. Sci. Total Environ. 626, 1295–1309. https://doi.org/10.1016/j.scitotenv.2018.01.066.

Abramenko, N., Kustov, L., Metelytsia, L., Kovalishyn, V., Tetko, I., Peijnenburg, W., 2020. A review of recent advances towards the development of QSAR models for toxicity assessment of ionic liquids. J. Hazard. Mater. 384, 121429 https://doi.org/10.1016/j.jhazmat.2019.121429.

Agathokleous, E., Liu, C.J., Calabrese, E.J., 2023a. Applications of the hormesis concept in soil and environmental health research. Soil Environ. Heal. 1, 100003 https://doi.org/10.1016/j.seh.2023.100003.

Agathokleous, E., Barceló, D., Calabrese, E.J., 2023b. A critical scientific and policy opinion on reuse and reclamation of contaminated wastewater for agriculture and other purposes. J. Environ. Chem. Eng. 11, 109352 https://doi.org/10.1016/j.jece.2023.109352.

Algamal, Z.Y., Qasim, M.K., Lee, M.H., Ali, H.T.M., 2020. High-dimensional QSAR/QSPR classification modeling based on improving pigeon optimization algorithm. Chemom. Intell. Lab. 206, 104170 https://doi.org/10.1016/j.chemolab.2020.104170.

Bai, Y.-B., Shi, M.-Y., Wang, W.-W., Wu, L.-Y., Bai, Y.-T., Li, B., Zhou, X.-Z., Zhang, J.-Y., 2022. Novel quorum sensing inhibitor Echinatin as an antibacterial synergist against *Escherichia coli*. Front. Microbiol. 13, 1003692. https://doi.org/10.3389/fmicb.2022.1003692.

Bernabè, G, Dal, Pra. M., Ronca, V., Pauletto, A., Marzaro, G., Saluzzo, F., Stefani, A., Artusi, I., De Filippis, V., Ferlin, M.G., 2021. A novel aza-derivative inhibits *agr* quorum sensing signaling and synergizes methicillin-resistant *Staphylococcus aureus* to clindamycin. Front. Microbiol. 12, 610859. Doi: 10.3389/fmicb.2021.610859.

Calabrese, E.J., Tsatsakis, A., Agathokleous, E., Giordano, J., Calabrese, V., 2020. Does green tea induce hormesis? Dose-Response. 18, 1559325820936170. Doi: 10.1177/1559325820936170.

Cao, J., Pan, Y., Jiang, Y., Qi, R., Yuan, B., Jia, Z., Jiang, J., Wang, Q., 2020. Computer-aided nanotoxicology: risk assessment of metal oxide nanoparticles via nano-QSAR. Green Chem. 22, 3512–3521. https://doi.org/10.1039/D0GC00933D.

Carradori, S., Di Giacomo, N., Lobefalo, M., Luisi, G., Campestre, C., Sisto, F., 2020. Biofilm and quorum sensing inhibitors: The road so far. Expert Opin. Ther. Pat. 30, 917–930. https://doi.org/10.1080/13543776.2020.1830059.

Chatterjee, M., Roy, K., 2021. Prediction of aquatic toxicity of chemical mixtures by the QSAR approach using 2D structural descriptors. J. Hazard. Mater. 408, 124936 https://doi.org/10.1016/j.jhazmat.2020.124936.

Cheng, Z., Chen, Q., Liu, S., Liu, Y., Ren, Y., Zhang, X., Shen, Z., 2022. The investigation of influencing factors on the degradation of sulfonamide antibiotics in iron-impregnated biochar-activated urea-hydrogen peroxide system: A QSAR study. J. Hazard. Mater. 430, 128269 https://doi.org/10.1016/j.jhazmat.2022.128269.

Cheong, M.S., Seo, K.H., Chohra, H., Yoon, Y.E., Choe, H., Kantharaj, V., Lee, Y.B., 2020. Influence of sulfonamide contamination derived from veterinary antibiotics on plant growth and development. Antibiotics. 9, 456. https://doi.org/10.3390/antibiotics9080456.

Cui, T., Bai, F., Sun, M., Lv, X., Li, X., Zhang, D., Du, H., 2020. Lactobacillus crustorum ZHG 2–1 as novel quorum-quenching bacteria reducing virulence factors and biofilms formation of Pseudomonas aeruginosa. LWT-Food Sci. Technol. 117, 108696 https://doi.org/10.1016/j.lwt.2019.108696.

Darby, E.M., Trampari, E., Siasat, P., Gaya, M.S., Alav, I., Webber, M.A., Blair, J.M., 2023. Molecular mechanisms of antibiotic resistance revisited. Nat. Rev. Microbiol. 21, 280–295. https://doi.org/10.1038/s41579-022-00820-y.

Díaz, M.A., González, S.N., Alberto, M.R., Arena, M.E., 2020. Human probiotic bacteria attenuate *Pseudomonas aeruginosa* biofilm and virulence by quorum-sensing inhibition. Biofouling. 36, 597–609. https://doi.org/10.1080/08927014.2020.1783253.

Fan, L., Huang, Y., Huang, T., Zhao, K., Zhang, Y.-N., Li, C., Zhao, Y.H., 2020. Photolysis and photo-induced toxicity of pyraclostrobin to *Vibrio fischeri*: Pathway and toxic mechanism. Aquat. Toxicol. 220, 105417 https://doi.org/10.1016/j.aquatox.2020.105417.

Giuliani, G., Melaccio, F., Gozem, S., Cappelli, A., Olivucci, M., 2021. QM/MM investigation of the spectroscopic properties of the fluorophore of bacterial luciferase. J. Chem. Theory Comput. 17, 605–613. https://doi.org/10.1021/acs.jctc.0c01078.

Golbraikh, A., Tropsha, A., 2002. Beware of q2! J. Mol. Graph. Model. 20, 269–276. https://doi.org/10.1016/S1093-3263(01)00123-1.

Gupta, S., Singh, A.K., Kushwaha, P.P., Prajapati, K.S., Shuaib, M., Senapati, S., Kumar, S., 2021. Identification of potential natural inhibitors of SARS-CoV2 main protease by molecular docking and simulation studies. J. Biomol. Struct. Dyn. 39, 4334–4345. https://doi.org/10.1080/07391102.2020.1776157.

Hamid, N., Junaid, M., Pei, D.-S., 2020. Individual and combined mechanistic toxicity of sulfonamides and their implications for ecological risk assessment in the Three Gorges Reservoir Area (TGRA). China. J. Hazard. Mater. 382, 121106 https://doi.org/10.1016/j.jhazmat.2019.121106.

Haque, M., Islam, S., Sheikh, M.A., Dhingra, S., Uwambaye, P., Labricciosa, F.M., Iskandar, K., Charan, J., Abukabda, A.B., Jahan, D., 2021. Quorum sensing: a new prospect for the management of antimicrobial-resistant infectious diseases. Expert Rev. Anti-Infe. 19, 571–586. https://doi.org/10.1080/14787210.2021.1843427.

Husain, A., Khan, S.A., Iram, F., Iqbal, M.A., Asif, M., 2019. Insights into the chemistry and therapeutic potential of furanones: A versatile pharmacophore. Eur. J. Med. Chem. 171, 66–92. https://doi.org/10.1016/j.ejmech.2019.03.021.

Jeelan, B.N., Basavarajaiah, S.M., Shyamsunder, K., 2022. Therapeutic potential of pyrrole and pyrrolidine analogs: an update. Mol. Divers. 26, 2915–2937. https://doi.org/10.1007/s11030-022-10387-8.

Kalia, V.C., 2013. Quorum sensing inhibitors: An overview. Biotechnol. Adv. 31, 224–245. https://doi.org/10.1016/j.biotechadv.2012.10.004.

Kalia, V.C., Patel, S.K.S., Kang, Y.C., Lee, J.-K., 2019. Quorum sensing inhibitors as antipathogens: biotechnological applications. Biotechnol. Adv. 37, 68–90. https://doi.org/10.1016/j.biotechadv.2018.11.006.

Kergoat, L., Besse-Hoggan, P., Leremboure, M., Beguet, J., Devers, M., Martin-Laurent, F., Masson, M., Morin, S., Roinat, A., Pesce, S., Bonnineau, C., 2021. Environmental concentrations of sulfonamides can alter bacterial structure and induce diatom deformities in freshwater biofilm communities. Front. Microbiol. 12, 643719 https://doi.org/10.3389/fmicb.2021.643719.

Kim, D.-S., Choi, J.-R., Ko, J., Kim, K., 2018. Re-engineering of bacterial luciferase; for new aspects of bioluminescence. Curr. Protein Pept. Sci. 19, 16–21. https://doi.org/10.2174/1389203718666161122104530.

Kulik, K., Lenart-Boroń, A., Wyrzykowska, K., 2023. Impact of antibiotic pollution on the bacterial population within surface water with special focus on mountain rivers. Water. 15, 975. https://doi.org/10.3390/w15050975.

Kumari, M., Kumar, A., 2020. Identification of component-based approach for prediction of joint chemical mixture toxicity risk assessment with respect to human health: A critical review. Food Chem. Toxicol. 143, 111458 https://doi.org/10.1016/j.fct.2020.111458.

Landi, C., Liberatori, G., Cotugno, P., Sturba, L., Vannuccini, M.L., Massari, F., Miniero, D.V., Tursi, A., Shaba, E., Behnisch, P.A., Carleo, A., Di Giuseppe, F., Angelucci, S., Bini, L., Corsi, I., 2022. First attempt to couple proteomics with the *AhR* reporter gene bioassay in soil pollution monitoring and assessment. Toxics. 10, 9. https://doi.org/10.3390/toxics10010009.

Lavado, G.J., Baderna, D., Carnesecchi, E., Toropova, A.P., Toropov, A.A., Dorne, J.L.C. M., Benfenati, E., 2022. QSAR models for soil ecotoxicity: Development and validation of models to predict reproductive toxicity of organic chemicals in the collembola *Folsomia candida*. J. Hazard. Mater. 423, 127236 https://doi.org/10.1016/j.jhazmat.2021.127236.

Li, X., Liu, Y., Wang, Y., Lin, Z., Wang, D., Sun, H., 2021. Resistance risk induced by quorum sensing inhibitors and their combined use with antibiotics: Mechanism and its relationship with toxicity. Chemosphere. 265, 129153 https://doi.org/10.1016/j.chemosphere.2020.129153.

Mangal, S., Chhibber, S., Singh, V., Harjai, K., 2022. Guaiacol augments quorum quenching potential of ciprofloxacin against *Pseudomonas aeruginosa*. J. Appl. Microbiol. 133, 2235–2254. https://doi.org/10.1111/jam.15787.

Mirjani, M., Soleimani, M., Salari, V., 2021. Toxicity assessment of total petroleum hydrocarbons in aquatic environments using the bioluminescent bacterium *Aliivibrio*

fischeri. Ecotox. Environ. Safe. 207, 111554 https://doi.org/10.1016/j.ecoenv.2020.111554.
Nandi, S., Ahmed, S., Saxena, A.K., 2018. Combinatorial design and virtual screening of potent anti-tubercular fluoroquinolone and isothiazoloquinolone compounds utilizing QSAR and pharmacophore modelling. SAR QSAR Environ. Res. 29, 151–170. https://doi.org/10.1080/1062936x.2017.1419375.
Naveira, C., Rodrigues, N., Santos, F.S., Santos, L.N., Neves, R.A., 2021. Acute toxicity of Bisphenol A (BPA) to tropical marine and estuarine species from different trophic groups. Environ. Pollut. 268, 115911 https://doi.org/10.1016/j.envpol.2020.115911.
Ning, Q., Wang, D., You, J., 2021. Joint effects of antibiotics and quorum sensing inhibitors on resistance development in bacteria. Environ. Sci.- Proc. Imp. 23, 995–1005. https://doi.org/10.1039/D1EM00047K.
Odularu, A.T., Afolayan, A.J., Sadimenko, A.P., Ajibade, P.A., Mbese, J.Z., 2022. Multidrug-resistant biofilm, quorum sensing, quorum quenching, and antibacterial activities of indole derivatives as potential eradication approaches. BioMed Res. Int. 2022, 9048245. https://doi.org/10.1155/2022/9048245.
Pan, F., Li, J., Zhao, L., Tuersuntuoheti, T., Mehmood, A., Zhou, N., Hao, S., Wang, C., Guo, Y., Lin, W., 2021. A molecular docking and molecular dynamics simulation study on the interaction between cyanidin-3-O-glucoside and major proteins in cow's milk. J. Food Biochem. 45, e13570.
Parvez, S., Venkataraman, C., Mukherji, S., 2006. A review on advantages of implementing luminescence inhibition test (Vibrio fischeri) for acute toxicity prediction of chemicals. Environ. Int. 32, 265–268. https://doi.org/10.1016/j.envint.2005.08.022.
Peng, D., Picchioni, F., 2020. Prediction of toxicity of ionic liquids based on GC-COSMO method. J. Hazard. Mater. 398, 122964 https://doi.org/10.1016/j.jhazmat.2020.122964.
Rezzoagli, C., Archetti, M., Mignot, I., Baumgartner, M., Kümmerli, R., 2020. Combining antibiotics with antivirulence compounds can have synergistic effects and reverse selection for antibiotic resistance in *Pseudomonas aeruginosa*. PLoS Biol. 18, e3000805.
Shao, Y., Wang, Y., Yuan, Y., Xie, Y., 2021. A systematic review on antibiotics misuse in livestock and aquaculture and regulation implications in China. Sci. Total Environ. 798, 149205 https://doi.org/10.1016/j.scitotenv.2021.149205.
Shen, H., Liu, Y., Liu, Y., Duan, Z., Wu, P., Lin, Z., Sun, H., 2021. Hormetic dose-responses for silver antibacterial compounds, quorum sensing inhibitors, and their binary mixtures on bacterial resistance of *Escherichia coli*. Sci. Total Environ. 786, 147464 https://doi.org/10.1016/j.scitotenv.2021.147464.
Stubblefield, W.A., Van Genderen, E., Cardwell, A.S., Heijerick, D.G., Janssen, C.R., De Schamphelaere, K.A., 2020. Acute and chronic toxicity of cobalt to freshwater organisms: using a species sensitivity distribution approach to establish international water quality standards. Environ. Toxicol. Chem. 39, 799–811. https://doi.org/10.1002/etc.4662.
Sun, H., Calabrese, E.J., Zheng, M., Wang, D., Pan, Y., Lin, Z., Liu, Y., 2018. A swinging seesaw as a novel model mechanism for time-dependent hormesis under dose-dependent stimulatory and inhibitory effects: A case study on the toxicity of antibacterial chemicals to *Aliivibrio fischeri*. Chemosphere. 205, 15–23. https://doi.org/10.1016/j.chemosphere.2018.04.043.
Sun, H., Chen, R., Jiang, W., Chen, X., Lin, Z., 2019. QSAR-based investigation on antibiotics facilitating emergence and dissemination of antibiotic resistance genes: A case study of sulfonamides against mutation and conjugative transfer in *Escherichia coli*. Environ. Res. 173, 87–96. https://doi.org/10.1016/j.envres.2019.03.020.
Sun, H., Pan, Y., Chen, X., Jiang, W., Lin, Z., Yin, C., 2020. Regular time-dependent cross-phenomena induced by hormesis: a case study of binary antibacterial mixtures to *Aliivibrio fischeri*. Ecotox. Environ. Safe. 187, 109823 https://doi.org/10.1016/j.ecoenv.2019.109823.
Szucs, R., Brown, R., Brunelli, C., Hradski, J., Masár, M., 2023. Impact of structural similarity on the accuracy of retention time prediction. J. Chromatogr. a. 1707, 464317 https://doi.org/10.1016/j.chroma.2023.464317.
Tang, L., Yang, M., Zhang, Y., Sun, H., 2022. Hormesis-based cross-phenomenon in judging joint toxic action for mixed pollutants. Curr. Opin. Environ. Sci. Health. 28, 100372 https://doi.org/10.1016/j.coesh.2022.100372.
Tian, D., Lin, Z., Yin, D., 2013. Quantitative structure activity relationships (QSAR) for binary mixtures at non-equitoxic ratios based on toxic ratios-effects curves. Dose-Response. 11, 255–269. https://doi.org/10.2203/dose-response.11-042.Lin.
Tian, Q., Wu, J., Xu, H., Hu, Z., Huo, Y., Wang, L., 2022. Cryo-EM structure of the fatty acid reductase LuxC–LuxE complex provides insights into bacterial bioluminescence. J. Biol. Chem. 298, 102006 https://doi.org/10.1016/j.jbc.2022.102006.
Tinikul, R., Chaiyen, P., 2016. Structure, mechanism, and mutation of bacterial luciferase. Adv. Biochem. Eng. Biot. 2016, 47–74. https://doi.org/10.1007/10_2014_281.
Wang, T., Liu, Y., Wang, D., Lin, Z., An, Q., Yin, C., Liu, Y., 2016. The joint effects of sulfonamides and quorum sensing inhibitors on *Vibrio fischeri*: Differences between the acute and chronic mixed toxicity mechanisms. J. Hazard. Mater. 310, 56–67. https://doi.org/10.1016/j.jhazmat.2016.01.061.
Wang, D., Shi, J., Xiong, Y., Hu, J., Lin, Z., Qiu, Y., Cheng, J., 2018a. A QSAR-based mechanistic study on the combined toxicity of antibiotics and quorum sensing inhibitors against *Escherichia coli*. J. Hazard. Mater. 341, 438–447. https://doi.org/10.1016/j.jhazmat.2017.07.059.
Wang, J., Wang, S., 2021. Toxicity changes of wastewater during various advanced oxidation processes treatment: An overview. J. Clean. Prod. 315, 128202 https://doi.org/10.1016/j.jclepro.2021.128202.
Wang, D., Wu, X., Lin, Z., Ding, Y., 2018b. A comparative study on the binary and ternary mixture toxicity of antibiotics towards three bacteria based on QSAR investigation. Environ. Res. 162, 127–134. https://doi.org/10.1016/j.envres.2017.12.015.
Wylie, A., Korchevskiy, A., 2022. Letter to the Editor: Epidemiology holds a key to the validation of toxicological models for elongate mineral particles. Curr. Res. Toxicol. 3, 100062 https://doi.org/10.1016/j.crtox.2021.100062.
Xiao, R., Ye, T., Wei, Z., Luo, S., Yang, Z., Spinney, R., 2015. Quantitative structure–activity relationship (QSAR) for the oxidation of trace organic contaminants by sulfate radical. Environ. Sci. Technol. 49, 13394–13402. https://doi.org/10.1021/acs.est.5b03078.
Yang, J., Wang, S., Zhang, T., Sun, Y., Han, L., Banahene, P.O., Wang, Q., 2021. Predicting the potential toxicity of 26 components in *Cassiae* semen using *in silico* and *in vitro* approaches. Curr. Res. Toxicol. 2, 237–245. https://doi.org/10.1016/j.crtox.2021.06.001.
Yang, S., Xu, F., Wu, F., Wang, S., Zheng, B., 2014. Development of PFOS and PFOA criteria for the protection of freshwater aquatic life in China. Sci. Total Environ. 470, 677–683. https://doi.org/10.1016/j.scitotenv.2013.09.094.
Yao, W.H., Mo, L.Y., Fang, L.S., Qin, L.T., 2023. Molecular dynamics simulations on interactions of five antibiotics with luciferase of *Vibrio Qinghaiensis* sp.-Q67. Ecotox. Environ. Safe. 256, 114910. Doi: 10.1016/j.ecoenv.2023.114910.
You, R., Sun, H., Yu, Y., Lin, Z., Qin, M., Liu, Y., 2016. Time-dependent hormesis of chemical mixtures: a case study on sulfa antibiotics and a quorum-sensing inhibitor of *Vibrio fischeri*. Environ. Toxicol. Phar. 41, 45–53. https://doi.org/10.1016/j.etap.2015.10.013.
Zhou, L., Zhang, Y., Ge, Y., Zhu, X., Pan, J., 2020. Regulatory mechanisms and promising applications of quorum sensing-inhibiting agents in control of bacterial biofilm formation. Front. Microbiol. 11, 589640 https://doi.org/10.3389/fmicb.2020.589640.
Zhu, X., Wu, G., Xing, Y., Wang, C., Yuan, X., Li, B., 2020. Evaluation of single and combined toxicity of bisphenol A and its analogues using a highly-sensitive micro-biosensor. J. Hazard. Mater. 381, 120908 https://doi.org/10.1016/j.jhazmat.2019.120908.
Zou, X., Lin, Z., Deng, Z., Yin, D., Zhang, Y., 2012. The joint effects of sulfonamides and their potentiator on *Photobacterium phosphoreum*: Differences between the acute and chronic mixture toxicity mechanisms. Chemosphere. 86, 30–35. https://doi.org/10.1016/j.chemosphere.2011.08.046.
Zuo, X.-L., Ai-yun, H., 2021. The residues and risk assessment of sulfonamides in animal products. J. Food Qual. 2021, 5597755. https://doi.org/10.1155/2021/5597755.